analytical chemistry

Article

Cite This: Anal. Chem. 2019, 91, 16002−16009

pubs.acs.org/ac

Ultrasensitive Electrochemical DNA Biosensor Based on a Label-Free Assembling Strategy Using a Triblock polyA DNA Probe

Lele Wang,[†] Yanli Wen,[†] Xue Yang,[†] Li Xu,[†] Wen Liang,[†] Ying Zhu,[§,∥] Lihua Wang,[§,∥] Yan Li,[‡] Yuan Li,[†] Min Ding,[†] Shuzhen Ren,[†] Zhenzhou Yang,[†] Min Lv,[§,∥] Jichao Zhang,*[,§,∥] Kang Ma,*[,‡] and Gang Liu*[,†]

[†]Laboratory of Biometrology, Division of Chemistry, Shanghai Institute of Measurement and Testing Technology, 1500 Zhang Heng Road, Shanghai 201203, People's Republic of China

[‡]Division of Chemical Metrology and Analytical Science, National Institute of Metrology of China, Beijing 102200, People's Republic of China

[§]Division of Physical Biology & Bioimaging Center, Shanghai Synchrotron Radiation Facility, CAS Key Laboratory of Interfacial Physics and Technology, Shanghai Institute of Applied Physics, Chinese Academy of Sciences, Shanghai 201800, People's Republic of China

[∥]Shanghai Advanced Research Institute, Chinese Academy of Sciences, Shanghai 201210, People's Republic of China

Supporting Information

ABSTRACT: Multiblock DNA probe attracted a large amount of scientific attention, for the development of multitarget biosensor and improved specificity/sensitivity. However, the development of multiblock DNA probes highly relied on the chemical synthesis of organic linkers or nanomaterials, which limited their practicability and biological compatibility. In this work, we developed a label-free assembling strategy using a triblock DNA capture probe, which connects two DNA probes with its intrinsic polyA fragment (probe−PolyA−probe, PAP). The middle polyA segment has a high affinity to the gold electrode surface, leading to excellent reproducibility, stability, and regeneration of our biosensor. Two flanking capture probes were tandemly co-assembled on the electrode surface with consistent spatial relationship and exactly the same amount. When combined with the target DNA, the hybridization stability was improved, because of the strong base stacking effect of two capture probes. The sensitivity of our biosensor was proved to be 10 fM, with a wide analysis range between 10 fM to 1 nM. Our PAP-based biosensor showed excellent specificity when facing mismatched DNA sequences. Even single nucleotide polymorphisms can be distinguished by each probe. The excellent practicability of our biosensor was demonstrated by analyzing genomic DNA both with and without PCR amplification.

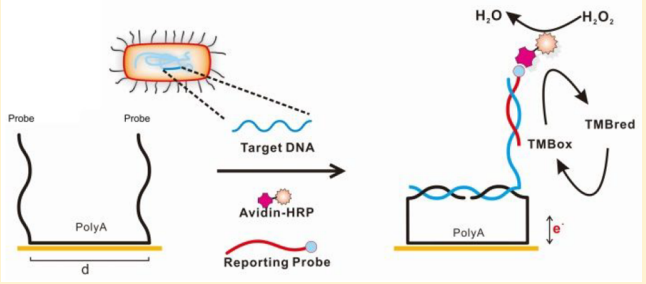

The DNA biosensor[1−6] has been widely recognized as a powerful tool for analysis activity in areas such as diagnosis,[7−10] food safety,[11] environment analysis,[12] biological antiterrorism, and basic research in life science,[13,14] showing advantages including on-site and real-time detection, low time/economical cost, and high sensitivity. In the development of biosensors, DNA probes[15−17] are playing a critical role. The linear DNA molecule has both interesting physicochemical properties, because of its own hydrophobic and hydrophilic groups and other chemical modifications. Furthermore, DNA provides a specific affinity toward a wide range of biological and chemical targets.[18−20] Thus, the DNA molecule was widely applied as an excellent material of the construction of probes toward various applications.

More recently, the development of multifunctional DNA[21] probes has drawn considerable research interest, for improved multitarget assay, nuclease resistance aptamer,[22] or higher specificity/affinity. One strategy for the construction of a multifunctional DNA probe was DNA-Au Biobarcode,[23−26] based on the co-assembling of DNA probes on Au nanoparticles (AuNPs). However, several challenges still remain for the development of DNA-Au probes, including the controllability of DNA assembling on the interface nanoparticles and the biological compatibility of AuNPs.

Another method was of DNA−organic molecule−DNA (DOD)[27−29] architecture through the molecular building. In 2004, Immoos and his co-workers developed the first E-DNA biosensor based on a triblock DNA probe.[30] They designed a "two-piece" DNA-PEG-DNA probe with a 3′ thiol label and a 5′ redox-active ferrocene (Fc) group. When the ABA

Received: October 18, 2019
Accepted: November 20, 2019
Published: November 20, 2019

DOI: 10.1021/acs.analchem.9b04757
Anal. Chem. 2019, 91, 16002−16009

Table 1. DNA Sequences Information

name[a]	sequence (5′−3′)
$PA_{10}P$-1	GCGCTTTCCCACCAACACACACACAAAAAAAAAAAACACACACACATTGCCCGGCTTTCTT
$PA_{20}P$-1	GCGCTTTCCCACCAACACACACACAAAAAAAAAAAAAAAAAAAAAACACACACACATTGCCCGGCTTTCTT
$PA_{30}P$-1	GCGCTTTCCCACCAACACACACACAAAAAAAAAAAAAAAAAAAAAAAAAAAAAAAACACACACACATTGCCCGGCTTTCTT
SP-1	ATCAATTCCACAGTTTTCGC
$PA_{10}P$-2	TTGCCCGGCTTTCTTCACACACACAAAAAAAAAAAACACACACACATTCCACAGTTTTCGC
$PA_{20}P$-2	TTGCCCGGCTTTCTTCACACACACAAAAAAAAAAAAAAAAAAAAAACACACACACATTCCACAGTTTTCGC
$PA_{30}P$-2	TTCCACAGTTTTCGCCACACACACAAAAAAAAAAAAAAAAAAAAAAAAAAAAAAAACACACACACATTGCCCGGCTTTCTT
SP-2	GCGCTTTCCCACCAACGCTG
$PA_{10}P$-3	TTCCACAGTTTTCGCCACACACACAAAAAAAAAAAACACACACACATTCCCACCAACGCTG
$PA_{20}P$-3	TTCCACAGTTTTCGCCACACACACAAAAAAAAAAAAAAAAAAAAAACACACACACATTCCCACCAACGCTG
$PA_{30}P$-3	TTCCACAGTTTTCGCCACACACACAAAAAAAAAAAAAAAAAAAAAAAAAAAAAAAACACACACACATTCCCACCAACGCTG
SP-3	TTGCCCGGCTTTCTTGTAAC
target	GCGAAAACTGTGGAATTGATCAGCGTTGGTGGGAAAGCGCGTTACAAGAAAGCCGGGCAA
ss-CP	GCGCTTTCCCACCAACACACACACAAAAAAAAAAAAAAAAAAAAAAAAAAAAA
primer 1	GCGAAAACTGTGGAATTGAT
primer 2	TGATGCTCCATCACTTCCTG
5MS-1	GCGCTTT*G*CCACCAACACACACACAAAAAAAAAAAAAAAAAAAAAAAAAAAAAAAACACACACACATTGCCCGGCTTTCTT
5MS-3	GCGCT*A*TGCGACCAACACACACACAAAAAAAAAAAAAAAAAAAAAAAAAAAAAAAACACACACACATTGCCCGGCTTTCTT
5MS-5	GCG*GT*A*T*GCGAGCAACACACACACAAAAAAAAAAAAAAAAAAAAAAAAAAAAAAAACACACACACATTGCCCGGCTTTCTT
3MS-1	GCGCTTTCCCACCAACACACACACAAAAAAAAAAAAAAAAAAAAAAAAAAAAAAAACACACACACATTGCCCGCCTTTCTT
3MS-3	GCGCTTTCCCACCAACACACACACAAAAAAAAAAAAAAAAAAAAAAAAAAAAAAAACACACACACATTGCCGGCCATTCTT
3MS-5	GCGCTTTCCCACCAACACACACACAAAAAAAAAAAAAAAAAAAAAAAAAAAAAAAACACACACACATTGGCGGCCATACTT
MS-2	GCGCTTT*G*CCACCAACACACACACAAAAAAAAAAAAAAAAAAAAAAAAAAAAAAAACACACACACATTGCCCGCCTTTCTT
MS-6	GCGCT*A*TGCGACCAACACACACACAAAAAAAAAAAAAAAAAAAAAAAAAAAAAAAACACACACACATTGCCGGCCATTCTT

[a]PA_XP = PAP capture probes with different length of polyA; SP = signal probe; ss-CP = traditional single-strand DNA probe; MS = mismatched sequances.

structured probe was immobilized onto the electrode surface and hybridized with the target DNA, the distance between the 5′-terminal Fc and the electrode surface was decreased, generating an electrical signal due to the redox of Fc. The ABA probe-based E-DNA sensor was demonstrated to be convenient and reagentless. DNA−fluorophore−DNA was also reported for homogeneous hybridization assays using fluorescence spectroscopic analysis.[31] However, development of the ABA DNA probes is highly reliant on chemical synthesis[32] and, thus, limits their practicability economic cost and biological compatibility.

The development of polyA DNA assembling[33] provides us a novel strategy of multifunctional DNA probes. Different from traditional thiol-DNA probes, the label-free polyA probes anchors on gold electrode[34] through the covalent binding between adenines and the gold surface.[35] In 2003, the Tarlov group, for the first time, reported the adsorption of polyA single-stranded DNA (ssDNA) onto polycrystalline Au films.[36] They and co-workers studied the assembling of polyA DNA on a gold surface and exhibited the possibility of DNA hybridization sensing on polyA DNA interfaces.[37] Pei et al. then reported a polyA biosensor on gold nanoparticles (AuNPs).[38] More recently, our group studied the electron transfer on polyA-based electrochemical interfaces[39] and constructed reusable electrochemical biosensors.[40]

Our objective in this work is to construct a label-free triblock polyA DNA probe (probe−polyA−probe, PAP) on the electrochemical biosensor interface, which connects two DNA probes with its intrinsic polyA fragments. The polyA fragment in the middle can combine with the Au electrode surface to form a compact and well-ordered biosensing interface, and as a consequence, two flanking DNA capture probes are assembled onto the electrode with adjustable distance and the same amount. Two capture probes are designed to simultaneously hybridize with adjacent sequences of the *Escherichia coli* (*E. coli*) genomic DNA, so the hybridization stability was distinctively improved, because of the base stacking effect. Critical experiment conditions for polyA probe assembling were systematically studied, including the length of the polyA fragment and the conformation of the hybridization conjugate. Finally, target DNA amounts as low as 10 fM were detected, and even single nucleotide polymorphism was successfully distinguished.

EXPERIMENTAL SECTION

Materials. DNA oligonucleotides were synthesized and purified by Invitrogen Trading Co., Ltd. (Shanghai, China), and the sequence information is shown in Table 1. The bacterial genomic DNA extraction kit and MCH (6-Mercapto-1-hexanol) were obtained from Sigma−Aldrich (Shanghai, China). The TMB substrate (3,3′,5,5′-tetramethylbenzidine) was purchased from Neogen Corporation (Shanghai, China). Avidin-horseradish peroxidase (avidin-HRP) was purchased from eBioscience, Inc. (San Diego, CA), and its diluent buffer was purchased from Fitzgerald Industries International (Acton, MA). *E. coli Dh5α*, dNTP mixture, Ex Taq DNA polymerase, and 10× Ex Taq buffer were obtained from Takara Biotechnology Co., Ltd. (Dalian, China). *Enterococcus faecalis* (*E. faecalis*) strain was provided by the China Center of Industrial Culture Collection (Beijing, China). Potassium ferricyanide ($K_3[Fe(CN)_6]$) and potassium ferrocyanide ($K_4Fe(CN)_6{\cdot}3H_2O$) were acquired from China National Pharmaceutical Group Corporation (Shanghai, China). All the chemicals were of analytical grade and used without further purification. Ultrapure water was obtained from a Milli-Q water purification system with a resistivity of 18.2 MΩ cm.

DOI: 10.1021/acs.analchem.9b04757
Anal. Chem. 2019, 91, 16002−16009

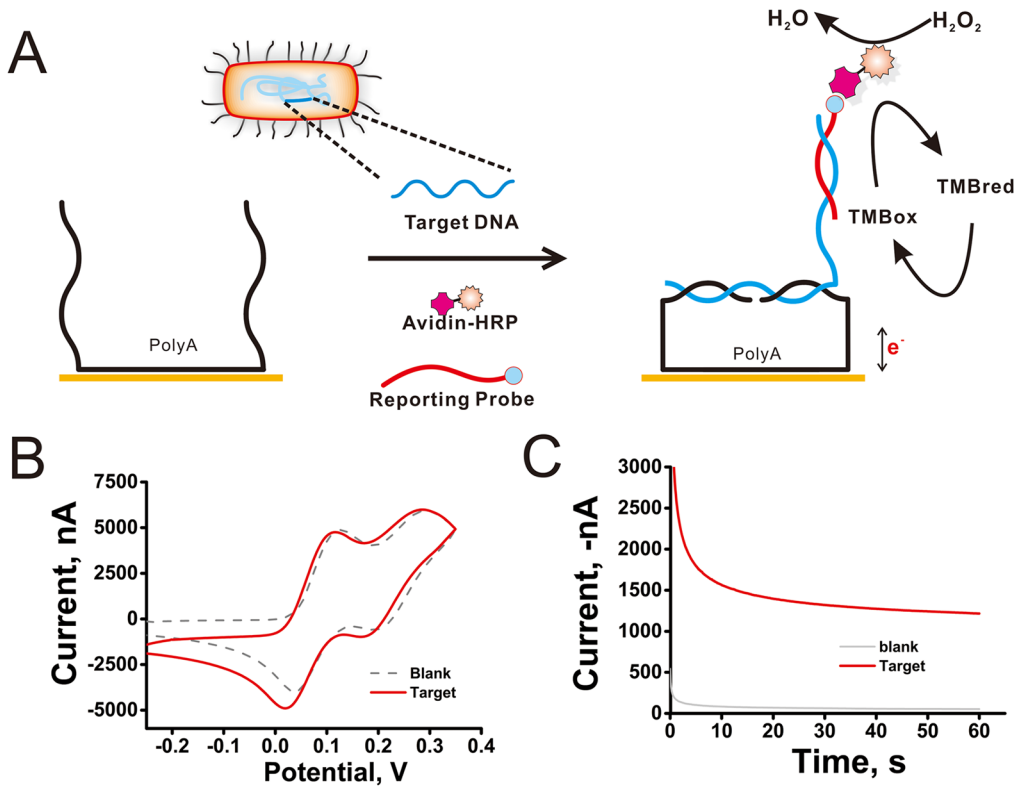

Figure 1. (A) Schematic illustration of the PAP-based electrochemical DNA biosensor and (B, C) analysis results in the absence of target DNA (panel B, CV circles, scan rate = 30 mV/s) and the presence of 1 nM target DNA (panel C, *I*–*t* curves, potential = −200 mV). $PA_{30}P$-1 was applied as the capture probe in this experiment.

Bacteria Culture and Genome Extraction. The bacteria strains (*E. coli DhSα* and *E. faecalis*) were grown in Luria broth (LB) medium at 37 °C overnight. The resultant bacterial cells were separated from the media by centrifuging at 6000 rpm for 5 min in a centrifuge (Eppendorf 5810R, Hamburg, Germany). A bacterial genomic DNA extraction kit then was utilized to extract bacterial genomic DNA.

PCR Amplification and Gel Electrophoresis Analysis. PCR amplification of genomic DNA was performed on a S1000 thermal cycler (Bio-Rad, USA). A pair of asymmetric primers (primer 1:primer 2 = 10:1) were employed to produce single-stranded DNA as many as possible. The PCR amplification procedure as follows: 95 °C, 2 min; 95 °C, 30 s, 61 °C, 30 s, 72 °C, 30 s, 50 cycles; 72 °C, 10 min; 4 °C, hold. The PCR products then were diluted to certain concentrations for gel electrophoresis analysis (Bio-Rad, USA). The electrophoresis was performed on 2% (w/w) agarose gel at a constant potential of 80 V for 40 min. After electrophoresis, the gel was visualized via a Gel Doc EZ imager system (Bio-Rad, USA).

Preparation of the PAP/MCH Electrode Surfaces. A 16-channel electrode array was used in our work, which has 16 groups of electrodes, and each group consisted of a round gold working electrode (2.3 mm diameter), a small square gold reference electrode, and a surrounding circle gold auxiliary electrode (see Figure S1 in the Supporting Information). 0.1 μM triblock polyA probe was added on electrochemical array electrodes. After being incubated overnight at room temperature, the probe-modified electrodes were blocked with 1 mM MCH for 30 min at room temperature. Unbound MCH was thoroughly washed away with Milli-Q water. Finally, the prepared electrodes were stored in a refrigerator (4–8 °C) before next step.

Electrochemical Measurement. A prehybridization solution (pH 7.4, 10 mM Tris·HCl, 1 mM EDTA, 1 M NaCl) containing 100 nM biotinylated reporter probe and certain concentration of target DNA was heated to 80 °C for 5 min and then cooled to room temperature for 20 min. The solution then was added onto the PAP-covered electrodes under 37 °C for 2 h. After hybridization, the electrodes were incubated with 5 U/mL avidin-HRP for 15 min at room temperature. Lastly, the electrodes were thoroughly rinsed with the washing buffer (pH 7.4, 10 mM Tris-HCl, 1 mM EDTA, 1 M NaCl) and subjected to electrochemical measurements.

Cyclic voltammetry (CV) measurement and amperometric measurement were performed in TMB substrate using the multichannel electrochemical workstation (Fasteur, China). The scan rate of CV was 30 mV/s. Amperometric detection was performed at −200 mV, and the electrocatalysis reduction current was recorded at 60 s after the HRP redox reaction reached the steady state. Electrochemical impedance spectroscopy (EIS) measurement was performed by an electrochemical workstation (μAUTOLAB III, Metrohm, Switzerland) and a conventional three-electrode system, which contained an Ag/AgCl reference electrode, a Pt counter electrode, and a gold working electrode. The EIS measurement solution was 5 mM $Fe(CN)_6^{3-/4-}$ and 0.1 M KCl in 10 mM PBS (pH 7.4). The AC voltage amplitude was 5 mV, and the voltage frequencies ranged from 0.01 Hz to 100 kHz.

DOI: 10.1021/acs.analchem.9b04757
Anal. Chem. 2019, 91, 16002–16009

RESULTS AND DISCUSSION

Construction of the PAP-Based Electrochemical Biosensor. In this study, the design and application of the polyA probe was dramatically extended. We developed a novel polyA triblock probe in an electrochemical biosensor (see Figure1). The probe was composed of a polyA sequence in the middle and two flanking capture probes at both ends (PAP). The polyA segment anchored on the gold electrode surface, and thus, these capture probes combined with the target DNA via specific hybridization on the electrode surface. A biotin-labeled signal probe (SP) then combined with the target DNA and captured an avidin-HRP, generating an electrochemical catalysis signal in a TMB substrate.

The electrochemical behavior of the PAP-based biosensor was investigated by CV measurement. As shown in Figure 1B, two well-defined redox peak pairs were obtained in the CV results, indicating excellent electron transfer between TMB and the gold electrode. The reduction peak at ~50 mV (vs a gold reference electrode) increased after the hybridization of 1 nM target DNA, because of the HRP catalysis electrochemical reaction. Amperometric measurement (Figure 1C) was then applied to collect the steady-state current signal, which is dependent on the target DNA concentration. The fabrication of the biosensor was characterized by electrochemical impedance spectroscopy (EIS). As shown in Figure 2, the bare gold electrode exhibited a very small charge transfer resistance, indicating a clean electrode surface (Figure 2A). When the PAP was immobilized on the electrodes, the EIS signal dramatically increased (Figure 2B,) because of the increased density of negative charge and consequently increased electrostatic repulsion for $[Fe(CN)_6]^{3-/4-}$ anions. As we expected, the EIS signal continued to increase step by step after the addition of MCH (Figure 2C), target DNA/reporter probe (Figure 2D), because of the gradually increased density of negative charge.

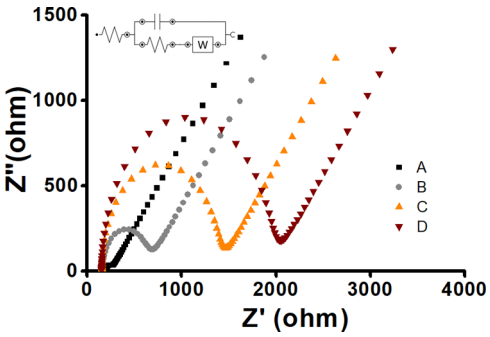

Figure 2. Nyquist plot of electrochemical impedance spectroscopy (EIS) measurements performed at different steps of the biosensor analysis: (A) bare gold electrode, (B) after PAP assembling (the length of polyA is 30 nt in this experiment), (C) after MCH passivation (PAP/MCH), (D) after addition of the hybridization solution (PAP/MCH/reporter probe/target). All the experiments were performed in 5 mM $K_3[Fe(CN)_6]/K_4[Fe(CN)_6]$ solution containing 0.1 M KCl. The concentration of the target DNA was 1 nM. $PA_{30}P$-1 was applied as the capture probe in this experiment.

Study of the PAP Assembling. PolyA sequence of different lengths (10, 20, 30, and 40 nt) were compared in the analysis of 1 nM target DNA. As shown in Figure 3A, when the length of polyA fragment increased from 10 nt to 30 nt, the current signal gradually increased while the blank signal decreased. The highest signal/noise ratio (S/N) (22.1) was achieved when the polyA sequence was 30 nt, which interestingly matched the length of the hybridization sequence in the target (30 nt) (Figure 1A). We attributed this phenomenon to the highest conformation stability of the hybridization conjugate on the electrochemical interface when the anchoring part perfectly matched the capturing part (Figure 1). However, when the length of polyA reached 40 nt, the current signal decreased dramatically, probably because the polyA40 probe occupied too much electrode surface and therefore affected the assembling amount of capture probes.

We then compared different PAP assembling for the analysis of the target DNA. We designed another type of capture probe ($PA_{30}P$-2 in Table 1), which hybridized with the target DNA at a different position. In the design of $PA_{30}P$-1, the reporter probe combined with the free 5′ end of the target sequence; in contrast, the reporter probe for $PA_{30}P$-2 strategy combined with the middle segment of the target DNA. As Figure 3B showed, the current signal of $PA_{30}P$-2 dramatically decreased, probably because the accessibility of the middle segment was limited due to the hybridization at two ends of the target DNA. An inverted reporter probe was also studied as a comparison. As the result showed (Figure 3B, $PA_{30}P$-3) the S/N dramatically decreased, because the biotin label was close to the electrode surface; thus, the increased steric hindrance affected the combination of avidin-HRP. Finally, the capture probe $PA_{30}P$-1 produced the highest S/N value, which was 1.8-fold higher than $PA_{30}P$-2 and 6.3-fold higher than $PA_{30}P$-3.

To achieve the best detection performance, several other critical experimental parameters were systematically optimized.

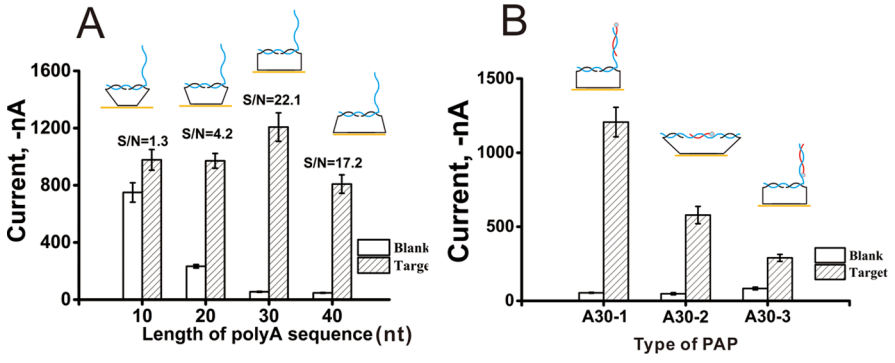

Figure 3. (A) Analysis results using PAP with different lengths of polyA (10, 20, 30, and 40 nt, respectively). (B) Analysis results using different types of capture probes. The concentration of the target DNA was 1 nM.

DOI: 10.1021/acs.analchem.9b04757
Anal. Chem. 2019, 91, 16002−16009

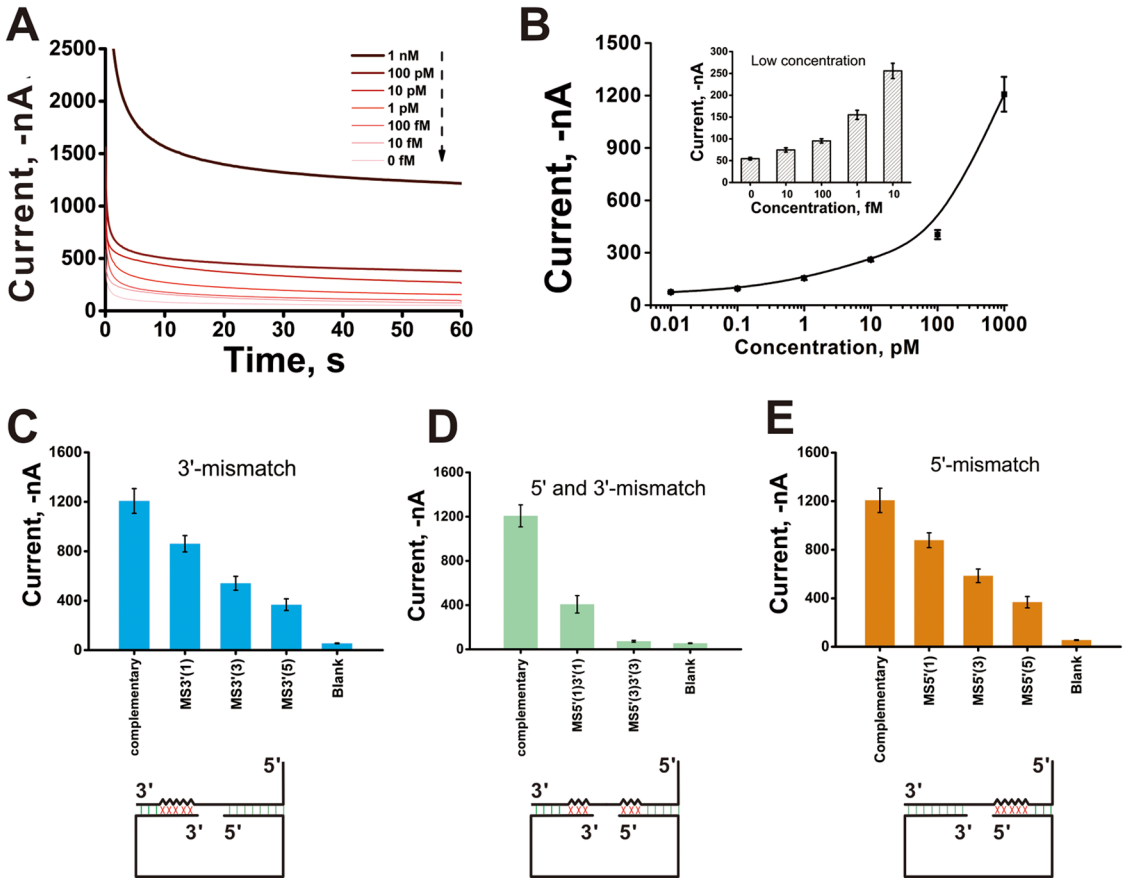

Figure 4. (A) *I*−*t* curves for a range of target DNA concentrations. From bottom to top: 0 fM, 10 fM, 100 fM, 1 pM, 10 pM, 100 pM, and 1 nM. The potential for *I*−*t* analysis was −200 mV. (B) Logarithmic plot of amperometric current vs target DNA concentrations (0−1 nM). The columns in the inset are the results of low concentration targets. (C) Mismatches at the 5′ end: MS5′(1), 1 mismatch; MS5′(3), 3 mismatches; MS5′(5), 5 mismatches. (D): Mismatches at 5′ and 3′ end: MS5′(1) 3′(1), 1 mismatch at both 5′ and 3′ end; MS5′(3) 3′(3), 3 mismatches at both 5′ and 3′ end. (E) Mismatches at 3′ end: MS3′(1), 1 mismatch; MS3′(3), 3 mismatches; MS3′(5), 5 mismatches. The concentration of the target DNA was 1 nM. The error bars represent standard deviations for measurements taken from at least three independent experiments.

(1) We optimized the concentration of PAP ($PA_{30}P$-1), which directly determined the density of capture probe on the electrode. The results showed that 0.1 μM PAP achieved the highest S/N value (Figure S2 in the Supporting Information).

(2) Next, we studied MCH passivation, which was proved to play a critical role in the construction of polyA-based biosensor.[39] As shown in Figure S3 in the Supporting Information, upon the addition of MCH, the background signal decreased dramatically as the deposition time increased from 10 min to 30 min, because MCH improved the resistance to the unspecific adsorption of DNA and enzyme. However, the S/N slightly decreased, probably because PAP was replaced on the electrode surface. Finally, 30 min was adopted as the optimized MCH deposition time in all of the following experiments.

(3) We then studied the signal probe concentration. As the results showed (see Figure S4 in the Supporting Information), 100 nM signal probe was finally demonstrated to be optimized for our biosensor.

(4) Finally, kinetics investigation showed the hybridization reaction reached a plateau after 2 h (Figure S5 in the Supporting Information); therefore, we performed 2 h of hybridization for the following analysis.

Performance of PAP Biosensor. *Sensitivity and Specificity.* The sensitivity of our biosensor was demonstrated by detecting a serial dilution of target DNA. *I*−*t* analysis curves (shown in Figure 4A) that the current signal increased with the increase of the target DNA concentration. The current signal at 60 s was taken as the quantification signal to construct a working curve with a target concentration from 10 fM to 1 nM (see Figure 4B). An excellent nonlinear fitting was finally achieved:

$$y = 270.7 - 196.7 \exp\left(-\frac{x}{3.36}\right)$$

where y is the current signal and x is the DNA concentration. The limit of detection (LOD) was demonstrated to be as low as 10 fM (see the inset of Figure 4B).

As a circle recognition probe, our PAP was anticipated to be capable of distinguishing mismatched DNA sequences. The specificity of our biosensor was systematically studied when facing a different number of mismatches at different positions (Figure 4 CDE). When 1, 2, or 3 mismatched bases were designed at 5′ end of the PAP capture probe, the current signal gradually decreased by ∼27.2%, 51.5%, and 69.5%, compared with a fully complementary sequence (see Figure 4C). A similar experimental result happened at the 3′ end of PAP (see Figure 4E). However, when the mismatched bases were designed at both the 5′ and 3′ terminal of PAP (Figure 4D), the current signal decreased much more significantly: 1

DOI: 10.1021/acs.analchem.9b04757
Anal. Chem. 2019, 91, 16002−16009

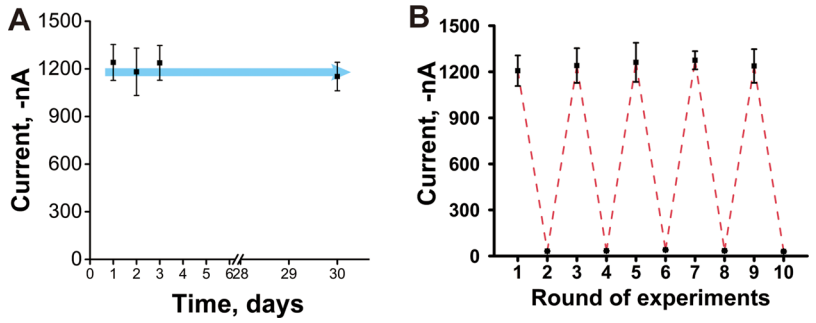

Figure 5. (A) Stability of the PAP-based biosensor. (B) Regeneration results of the PAP-based biosensor: 1, 3, 5, 7, and 9 were the detection steps, and 2, 4, 6, 8, 10 were the regeneration steps. The concentration of target DNA was 1 nM.

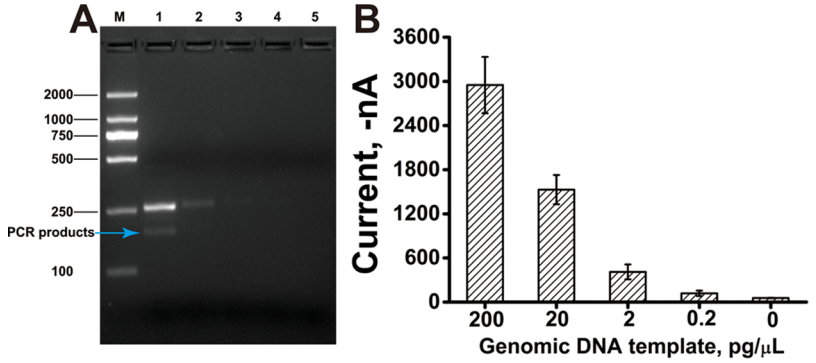

Figure 6. Analysis results of the asymmetric PCR product. The template was extracted and serially diluted *E. coli* genomic DNA. (A) Electrophoretic analysis of the PCR amplicons. The template concentrations were as follows: lane 1, 2 ng/μL; lane 2, 200 pg/μL; lane 3, 20 pg/μL; lane 4, 2 pg/μL; and lane 5, 0.2 pg/μL. Lane M is the marker. The final volume of the PCR solution is 10 μL. (B) Electrochemical detection of *E. coli* genomic DNA by using the PAP-based biosensor.

mismatch and 3 mismatches at both 5′ and 3′ end caused signal decreases of 66.2% and 94.0%, respectively. PAP recognized the target DNA with two probe segments, each probe showed excellent specificity. As the results showed, if the mismatches happened on two probes (MS5′(1)3′(1) in Figure 4D), the current signal was much lower than the situation on one probe (MS3′(3) in Figure 4D and MS5′(3) in Figure 4E), even with fewer mismatches.

Robustness of the PAP-Based Biosensor. Our biosensor was constructed on a 16-channel electrode array (see Figure S1). To challenge the reproducibility of our biosensors, 8 arrays were prepared at one time and then applied for the analysis of the same sample. As illustrated in Figure S6 in the Supporting Information, the relative standard deviation of measurements for the 8 sensor arrays was only 4.2%, indicating excellent reproducibility of our PAP-based biosensor.

The stability of our biosensor was also studied. The prepared electrode arrays after PAP assembling were stored under 4−8 °C for different time (2, 3, and 30 days) before being used. The current signal was collected and compared (Figure 5A). A highly repeatable current signal occurred after 3 days. Compared with the first electrode array, the one after 30 days of storage only decreased by ∼5%, demonstrating the good stability of our biosensor.

As reported in our previous work, the polyA-based assembling was stable enough to survive the hybridization melting process.[11] In this paper, the regeneration of our PAP was also studied. An electrode array modified with PAP was applied for the detection of 1 nM target DNA (Figure 5B, first round) and then treated with urea solution (8 M). As a result, in the regeneration step, the double-strand DNA (dsDNA) was fully denatured, and the signal probe was washed off to achieve the very low initial blank signal (Figure 5B, second round). Interestingly, the regenerated biosensor can be applied for another round of analysis, producing the same level of the current signal. The entire recycling process can be repeated at least five times.

The Practicability of the PAP-Based Biosensor. To prove the practicability, our PAP-based biosensor was applied to the analysis of a complex PCR product. First, the *E. coli* genome was extracted and amplified by asymmetric PCR to produce single-stranded target DNA as much as possible, and then the product was analysis both by agarose gel electrophoresis (Figure 6A) and our biosensor (Figure 6B). Finally, our biosensor successfully detected an unpurified PCR product from 0.2 pg/μL DNA template in 10 μL of solution. The sensitivity of our biosensor was proven to be 3 orders of magnitude higher than agarose gel electrophoresis.

As more-solid evidence of practicability, our biosensor was directly applied to the analysis of the *E. coli* genome without PCR amplification. The detection results show that the current signal of 10.0 pM *E. coli* genome was −283 nA, which was almost as high as synthetic target DNA of the same concentration. Meanwhile, the *E. faecalis* genome was prepared and analyzed as a negative control. 20.4 pM *E. faecalis* genome only exhibited a negligible current signal, which was close to the blank. This result demonstrated the excellent detection capability of our biosensor facing real samples (Figure 7).

■ CONCLUSIONS

In this work, we successfully developed a label-free nano-assembling strategy using a triblock DNA capture probe

DOI: 10.1021/acs.analchem.9b04757
Anal. Chem. 2019, 91, 16002−16009

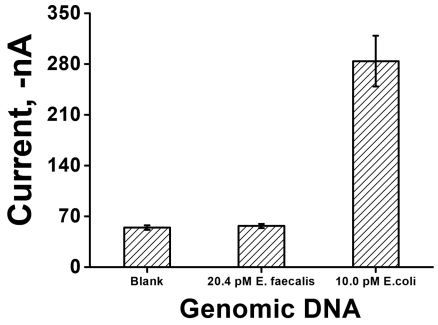

Figure 7. Analysis of *E. coli* genome and *E. faecalis* genome using our biosensor.

toward a sensitive electrochemical biosensor. The multifunctional DNA probe played a critical role in the construction of the biosensor. The middle polyA segment showed excellent assembling capability on the gold electrode surface, leading to improved reproducibility, stability, and regeneration of the biosensor. More importantly, two tandem capture probes were co-assembled on the electrode surface simultaneously, with consistent spatial position and exactly the same amounts. When combined with the target DNA, two capture probes generated strong base stacking effect, and thus improved the hybridization stability. The sensitivity of our biosensor was proved to be 10 fM, with a wide working range between 10 fM to 1 nM, which is quite comparable in recently reported works (see Table 2). Interestingly, our PAP-based biosensor showed

Table 2. Comparison of Our Biosensor with Some Reported Literature about *E. coli* Analysis

probe	renewability	dynamic range	limit of detection, LOD	ref
SH-DNA	not reported	0.37−10 nM	160 pM	41
SH-DNA	not reported	1 pM−10 nM	1 pM	42
amino-modified probe	not reported	1.0−70 pM	0.3 pM	43
DNA nanostructural probe	not reported	10 fM−10 nM	10 fM	44
molecular beacon	not reported	1−40 nM	0.17 nM	45
PAP	5 times	10 fM−1 nM	10 fM	this work

excellent specificity when facing mismatched DNA sequences. Even single nucleotide polymorphisms can be distinguished by each probe. The practicability of the PAP-based biosensor was demonstrated by analyzing genomic DNA both with and without PCR amplification. As a novel interface assembling strategy, the PAP method dramatically decreased the economic cost for the multifunctional DNA probe and the function can be conveniently extended by modifying the probe sequence. PAP not only showed unique advantages for the analysis of bacterial DNA: we believe it also opened a novel avenue for the development of multifunctional DNA probe for electrochemical biosensor.

■ ASSOCIATED CONTENT

Supporting Information

The Supporting Information is available free of charge at https://pubs.acs.org/doi/10.1021/acs.analchem.9b04757.

Schematic illustration of our 16-channel electrochemical array; optimization of the concentrations of polyA30 capture; optimization of the hybridization time; reproducibility of the polyA-tP based biosensor (PDF)

■ AUTHOR INFORMATION

Corresponding Authors

*E-mail: liug@simt.com.cn (G. Liu).
*E-mail: Makang@nim.ac.cn (K. Ma).
*E-mail: zjchao@sinap.ac.cn (J. Zhang).

ORCID

Lihua Wang: 0000-0002-6198-7561
Min Lv: 0000-0003-0587-8528
Gang Liu: 0000-0003-3779-7212

Notes

The authors declare no competing financial interest.

■ ACKNOWLEDGMENTS

This work was financially supported by The National Quality Infrastructure Program of China (No. 2018YFF0212800), National Natural Science Foundation of China (Nos. 21775104 and 11705270), The Youth Innovation Promotion Association of CAS (No. 2012205), The National Major Special Project for the Development of Transgenic Organisms (No. 2018ZX08011-04B), Shanghai Sailing Program (No. 17YF1423600).

■ REFERENCES

(1) Fan, C.; Wang, S.; Hong, J. W.; Bazan, G. C.; Plaxco, K. W.; Heeger, A. J. *Proc. Natl. Acad. Sci. U. S. A.* **2003**, *100*, 6297−6301.
(2) Su, S.; Sun, H.; Cao, W.; Chao, J.; Peng, H.; Zuo, X.; Yuwen, L.; Fan, C.; Wang, L. *ACS Appl. Mater. Interfaces* **2016**, *8*, 6826−6833.
(3) Zeng, D.; San, L.; Qian, F.; Ge, Z.; Xu, X.; Wang, B.; Li, Q.; He, G.; Mi, X. *ACS Appl. Mater. Interfaces* **2019**, *11*, 21859−21864.
(4) Zhang, J.; Song, S.; Zhang, L.; Wang, L.; Wu, H.; Pan, D.; Fan, C. *J. Am. Chem. Soc.* **2006**, *128*, 8575−8580.
(5) Liu, G.; Lao, R. J.; Xu, L.; Xu, Q.; Li, L. Y.; Zhang, M.; Shen, H.; Mathur, S.; Fan, C. H.; Song, S. P. *Sensors* **2011**, *11*, 8018−8027.
(6) Liu, G.; Wan, Y.; Zou, Z. Y.; Ren, S. Z.; Fan, C. H. *Chin. J. Anal. Chem.* **2011**, *39*, 953−962.
(7) Wen, Y. L.; Liu, G.; Pei, H.; Li, L. Y.; Xu, Q.; Liang, W.; Li, Y.; Xu, L.; Ren, S. Z.; Fan, C. H. *Methods* **2013**, *64*, 276−282.
(8) Yang, X.; Wen, Y. L.; Wang, L. L.; Zhou, C. Q.; Li, Q.; Xu, L.; Li, L. Y.; Shi, J. Y.; Lal, R.; Ren, S. Z.; Li, J.; Jia, N. Q.; Liu, G. *ACS Appl. Mater. Interfaces* **2017**, *9*, 38281−38287.
(9) Zeng, D.; Wang, Z.; Meng, Z.; Wang, P.; San, L.; Wang, W.; Aldalbahi, A.; Li, L.; Shen, J.; Mi, X. *ACS Appl. Mater. Interfaces* **2017**, *9*, 24118−24125.
(10) Deng, S.; Yan, J.; Wang, F.; Su, Y.; Zhang, X.; Li, Q.; Liu, G.; Fan, C.; Pei, H.; Wan, Y. *Biosens. Bioelectron.* **2019**, *137*, 263−270.
(11) Li, L. Y.; Wang, L. L.; Xu, Q.; Xu, L.; Liang, W.; Li, Y.; Ding, M.; Aldalbahi, A.; Ge, Z. L.; Wang, L. H.; Yan, J.; Lu, N.; Li, J.; Wen, Y. L.; Liu, G. *ACS Appl. Mater. Interfaces* **2018**, *10*, 6895−6903.
(12) Xiao, M.; Qu, X.; Li, L.; Pei, H. *Methods Mol. Biol.* **2018**, *1811*, 137−149.
(13) Song, P.; Li, M.; Shen, J.; Pei, H.; Chao, J.; Su, S.; Aldalbahi, A.; Wang, L.; Shi, J.; Song, S.; Wang, L.; Fan, C.; Zuo, X. *Anal. Chem.* **2016**, *88*, 8043−8049.
(14) Ye, D.; Li, L.; Li, Z.; Zhang, Y.; Li, M.; Shi, J.; Wang, L.; Fan, C.; Yu, J.; Zuo, X. *Nano Lett.* **2019**, *19*, 369−374.

DOI: 10.1021/acs.analchem.9b04757
Anal. Chem. 2019, 91, 16002−16009

(15) Li, D.; Song, S.; Fan, C. *Acc. Chem. Res.* **2010**, *43*, 631−641.
(16) Song, S.; Qin, Y.; He, Y.; Huang, Q.; Fan, C.; Chen, H. Y. *Chem. Soc. Rev.* **2010**, *39*, 4234−4243.
(17) Wang, X.; Hou, T.; Lu, T.; Li, F. *Anal. Chem.* **2014**, *86*, 9626−9631.
(18) Su, S.; Fan, J.; Xue, B.; Yuwen, L.; Liu, X.; Pan, D.; Fan, C.; Wang, L. *ACS Appl. Mater. Interfaces* **2014**, *6*, 1152−1157.
(19) Su, J.; Wang, D.; Nörbel, L.; Shen, J.; Zhao, Z.; Dou, Y.; Peng, T.; Shi, J.; Mathur, S.; Fan, C.; Song, S. *Anal. Chem.* **2017**, *89*, 2531−2538.
(20) Zhang, Z.; Zeng, D.; Ma, H.; Feng, G.; Hu, J.; He, L.; Li, C.; Fan, C. *Small* **2010**, *6*, 1854−1858.
(21) Lee, J. K.; Ko, S.; Bao, Z. *Macromol. Rapid Commun.* **2012**, *33*, 938−942.
(22) Kuai, H.; Zhao, Z.; Mo, L.; Liu, H.; Hu, X.; Fu, T.; Zhang, X.; Tan, W. *J. Am. Chem. Soc.* **2017**, *139*, 9128−9131.
(23) Hu, K.; Lan, D.; Li, X.; Zhang, S. *Anal. Chem.* **2008**, *80*, 9124−9130.
(24) Nam, J. M.; Thaxton, C. S.; Mirkin, C. A. *Science* **2003**, *301*, 1884−1886.
(25) Wang, Z.; Zhang, J.; Zhu, C.; Wu, S.; Mandler, D.; Marks, R. S.; Zhang, H. *Nanoscale* **2014**, *6*, 3110−3115.
(26) Boisselier, E.; Astruc, D. *Chem. Soc. Rev.* **2009**, *38*, 1759−1782.
(27) Lee, J. K.; Jung, Y. H.; Stoltenberg, R. M.; Tok, J. B. H.; Bao, Z. *J. Am. Chem. Soc.* **2008**, *130*, 12854−12855.
(28) Alemdaroglu, F. E.; Herrmann, A. *Org. Biomol. Chem.* **2007**, *5*, 1311−1320.
(29) Alemdaroglu, F. E.; Alemdaroglu, N. C.; Langguth, P.; Herrmann, A. *Adv. Mater.* **2008**, *20*, 899−902.
(30) Immoos, C. E.; Lee, S. J.; Grinstaff, M. W. *J. Am. Chem. Soc.* **2004**, *126*, 10814−10815.
(31) Ergen, E.; Weber, M.; Jacob, J.; Herrmann, A.; Mullen, K. *Chem. - Eur. J.* **2006**, *12*, 3707−3713.
(32) Lee, J. K.; Jung, Y. H.; Tok, J. B. H.; Bao, Z. *ACS Nano* **2011**, *5*, 2067−2074.
(33) Wang, L.; Zhang, H.; Wang, C.; Xu, Y.; Su, J.; Wang, X.; Liu, X.; Feng, D.; Wang, L.; Zuo, X.; Shi, J.; Ge, Z.; Fan, C.; Mi, X. *Biosens. Bioelectron.* **2019**, *127*, 85−91.
(34) Schreiner, S. M.; Shudy, D. F.; Hatch, A. L.; Opdahl, A.; Whitman, L. J.; Petrovykh, D. Y. *Anal. Chem.* **2010**, *82*, 2803−2810.
(35) Koo, K. M.; Carrascosa, L. G.; Shiddiky, M. J. A.; Trau, M. *Anal. Chem.* **2016**, *88*, 2000−2005.
(36) Kimura-Suda, H.; Petrovykh, D. Y.; Tarlov, M. J.; Whitman, L. J. *J. Am. Chem. Soc.* **2003**, *125*, 9014−9015.
(37) Opdahl, A.; Petrovykh, D. Y.; Kimura-Suda, H.; Tarlov, M. J.; Whitman, L. J. *Proc. Natl. Acad. Sci. U. S. A.* **2007**, *104*, 9−14.
(38) Pei, H.; Li, F.; Wan, Y.; Wei, M.; Liu, H.; Su, Y.; Chen, N.; Huang, Q.; Fan, C. *J. Am. Chem. Soc.* **2012**, *134*, 11876−11879.
(39) Li, L.; Wang, L.; Xu, Q.; Xu, L.; Liang, W.; Li, Y.; Ding, M.; Aldalbahi, A.; Ge, Z.; Wang, L.; Yan, J.; Lu, N.; Li, J.; Wen, Y.; Liu, G. *ACS Appl. Mater. Interfaces* **2018**, *10*, 6895−6903.
(40) Wang, Q.; Wen, Y.; Li, Y.; Liang, W.; Li, W.; Li, Y.; Wu, J.; Zhu, H.; Zhao, K.; Zhang, J.; Jia, N.; Deng, W.; Liu, G. *Anal. Chem.* **2019**, *91*, 9277−9283.
(41) Saeed, A. A.; Sanchez, J. L. A.; O'Sullivan, C. K.; Abbas, M. N. *Bioelectrochemistry* **2017**, *118*, 91−99.
(42) Zhang, J.; Lao, R.; Song, S.; Yan, Z.; Fan, C. *Anal. Chem.* **2008**, *80*, 9029−9233.
(43) Zhang, Y.; Geng, X.; Ai, J.; Gao, Q.; Qi, H.; Zhang, C. *Sens. Actuators, B* **2015**, *221*, 1535−1541.
(44) Wen, Y.; Wang, L.; Xu, L.; Li, L.; Ren, S.; Cao, C.; Jia, N.; Aldalbahi, A.; Song, S.; Shi, J.; Xia, J.; Liu, G.; Zuo, X. *Analyst* **2016**, *141*, 5304−5310.
(45) Gerasimova, Y. V.; Kolpashchikov, D. M. *Biosens. Bioelectron.* **2013**, *41*, 386−390.

DOI: 10.1021/acs.analchem.9b04757
Anal. Chem. 2019, 91, 16002−16009